Int. J. Heat Mass Transfer. Vol. 36, No. 14, pp. 3509–3514, 1993
Printed in Great Britain

0017–9310/93 $6.00+0.00

Heat and mass transfer through a liquid metal in an infinitely long, rotating cylinder with a uniform, transverse magnetic field

M. C. HALL and J. S. WALKER

Department of Mechanical and Industrial Engineering, University of Illinois at Urbana-Champaign, 1206 West Green St., Urbana, IL 61801, U.S.A.

(*Received* 16 *July* 1992 *and in final form* 29 *January* 1993)

Abstract—This paper treats a liquid-metal motion in an infinitely long, vertical cylinder which is rotating about its vertical axis in the presence of a steady, uniform, horizontal magnetic field. The liquid near the cylinder wall rotates with the cylinder, but elsewhere the velocity is parallel to the magnetic field. This paper also treats a steady, two-dimensional heat and mass transfer problem which qualitatively models some aspects of the Czochralski growth of silicon crystals with a uniform, horizontal magnetic field. In spite of the strongly asymmetric flow and relatively large values of the Peclet number, the temperature and solutal distributions do not deviate significantly from axisymmetry.

1. INTRODUCTION

IN THE Czochralski process, a single crystal of silicon is grown from molten silicon contained in a quartz (SiO_2) crucible. The melt motion is generally periodic or turbulent, and the resultant fluctuations in heat transfer from the melt to the crystal create a periodic cycle of crystallization and remelting. This cycle produces a relatively high microdefect density in the crystal [1]. Since molten silicon is an excellent electrical conductor, the application of a steady magnetic field during crystal growth suppresses turbulence and any other periodicity in the melt motion and thus reduces the microdefect density in the crystal [2, 3].

Most experiments and numerical simulations to date have focused on the effects of a steady, uniform magnetic field which is either vertical and parallel to the common vertical axis of the crystal and crucible (axial field) or is horizontal and perpendicular to this vertical axis (transverse field). Initially, axial fields seemed to be better because the melt motion, temperature and solutal distributions remain axisymmetric with an axial field. A transverse field which is strong enough to suppress turbulence also produces a large asymmetry in the melt motion. If the associated convective heat transfer produces a large asymmetry in the temperature, then a point on the face of the crystal, which is rotating about its vertical axis, will experience precisely the periodic fluctuations in heat transfer which the magnetic field is supposed to eliminate. However, experiments have revealed that crystals grown in an axial magnetic field have an unacceptably high and extremely non-uniform concentration of oxygen [4]. Oxygen enters the melt as the crucible is ablated during crystal growth. An axial magnetic field strongly suppresses the radially outward flow near the crystal face which is driven by the crystal rotation and which ensures radially uniform distributions of oxygen and other solutes in the crystal [5]. On the other hand, crystals grown in a uniform, transverse magnetic field have very uniform and controllable concentrations of oxygen and dopants, and do not have any of the undesirable characteristics which would be produced by large asymmetries in the temperature or solutal distributions in the melt [4, 6].

The objective of the present paper is to investigate the deviations from thermal and solutal axisymmetry associated with a strongly asymmetric fluid motion. We do not treat the complex, three-dimensional melt motion in the actual Czochralski process. Instead we treat a two-dimensional model problem which qualitatively reflects some aspects of the Czochralski process. The results cannot be used to make any quantitative predictions about the Czochralski process, but they do reveal that the asymmetries in the temperature and solutal distributions are much smaller than one might expect from the strongly asymmetric flow and from the magnitudes of the Peclet numbers considered. Therefore the results provide some insights into the lack of poor characteristics in crystals grown in a uniform transverse magnetic field.

Mihelcic and Wingerath [7] present numerical simulations of the fully three-dimensional melt motion and heat transfer in the Czochralski process with a uniform transverse magnetic field. However, they impose a strongly asymmetric temperature distribution with a hot spot on one side of the crucible and investigate the effects of a transverse magnetic field with various orientations with respect to the hot spot. Here we treat a heat transfer problem whose only asymmetry results from the application of the transverse field.

NOMENCLATURE

a dimensionless radius of the thermal and solutal sinks
A_{mn}, B_{mn}, C_{mn} coefficients in the Fourier–Chebyshev spectral series
B magnetic flux density of the uniform, horizontal magnetic field
Bi Biot number, hR^2/k
C concentration of the solute in the liquid metal
c_h specific heat of the liquid metal
D diffusion coefficient for the solute in the liquid metal
h or h_m heat or mass transfer coefficient for thermal or solutal sinks
Ha Hartmann number, $BR(\sigma/\mu)^{1/2}$
$H(x)$ Heaviside function 1 or 0 for $x > 0$ or $x < 0$, respectively
$\mathbf{j}$ dimensionless electric current density in the liquid metal
k thermal conductivity of the liquid metal
N interaction parameter, $\sigma B^2/\rho\Omega$
p dimensionless pressure in the liquid metal
Pe or Pe_m Peclet ($\rho c_h \Omega R^2/k$) or mass Peclet ($\Omega R^2/D$) number
q or q_m heat or mass flux at the vertical cylinder wall
R radius of the cylinder
R_m magnetic Reynolds number, $\mu_p \sigma \Omega R^2$
Sh Sherwood number, $h_m R^2/D$
T dimensionless temperature in the liquid metal
$T_k(x)$ Chebyshev polynomials
$\mathbf{v}$ dimensionless velocity in the liquid metal.

Greek symbols

μ absolute viscosity of the liquid metal
μ_p magnetic permeability of the liquid metal
ρ density of the liquid metal
ϕ dimensionless electric potential function
ψ stream function for the liquid-metal motion in horizontal planes
Ω angular velocity of cylinder's rotation about its vertical axis.

2. LIQUID-METAL MOTION

In this section we treat the steady motion of a liquid metal with constant physical properties in an infinitely long, vertical cylinder which is rotating about its vertical axis with an angular velocity Ω, as shown in Fig. 1. We use the cylindrical coordinates (r, θ, z) with the z axis along the cylinder's vertical axis and with the unit vectors $\hat{\mathbf{r}}, \hat{\boldsymbol{\theta}}, \hat{\mathbf{z}}$. There is a steady, uniform, externally applied, horizontal magnetic field, $B\hat{\mathbf{y}}$, where $\hat{\mathbf{y}} = \sin\theta\,\hat{\mathbf{r}} + \cos\theta\,\hat{\boldsymbol{\theta}}$ is a horizontal unit vector which is parallel to the radii at $\theta = \pm\pi/2$ and B is the magnetic flux density. In addition to the applied magnetic field, there is an induced magnetic field produced by the electric currents in the liquid metal. The characteristic ratio of the induced magnetic flux density to B is the magnetic Reynolds number $R_m = \mu_p \sigma \Omega R^2$, where μ_p and σ are the magnetic permeability and electrical conductivity of the liquid metal, while R is the inside radius of the cylinder. For molten silicon in a 20 cm diameter crucible rotating at 0.1 rad s^{-1}, $R_m = 0.00126$, so that we neglect the induced magnetic field.

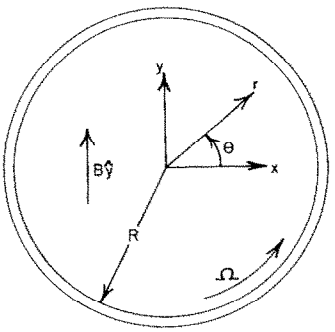

FIG. 1. Horizontal section of an infinitely long, vertical cylinder which is filled with a liquid metal and which is rotating about its vertical axis in the presence of a steady, uniform, horizontal, externally applied magnetic field $B\hat{\mathbf{y}}$.

In the momentum equation, the characteristic ratios of the electromagnetic (EM) body force to the inertial and viscous terms are N and Ha^2, respectively, where $N = \sigma B^2/\rho\Omega$ and $Ha = BR(\sigma/\mu)^{1/2}$ are the interaction parameter and Hartmann number, respectively. Here ρ and μ are the density and viscosity of the liquid metal. For our silicon example with $B = 0.2$ T, $N = 172$, which is sufficiently large to neglect inertial effects. Therefore the dimensionless equations governing the fluid motion are

$$0 = -\nabla p + \mathbf{j} \times \hat{\mathbf{y}} + Ha^{-2}\nabla^2 \mathbf{v}, \quad \nabla \cdot \mathbf{v} = 0, \quad \text{(1a,b)}$$

$$\mathbf{j} = -\nabla\phi + \mathbf{v} \times \hat{\mathbf{y}}, \quad \nabla \cdot \mathbf{j} = 0, \quad \text{(1c,d)}$$

where p, $\mathbf{j}$, $\mathbf{v}$ and ϕ are the pressure, electric current density, velocity and electric potential function, normalized by $\sigma\Omega R^2 B^2$, $\sigma\Omega R B$, ΩR and $\Omega R^2 B$, respectively. Equation (1a) is the inertialess momentum equation with the EM body force $\mathbf{j} \times \hat{\mathbf{y}}$ and equation (1c) is Ohm's law, while equations (1b) and (1d) guarantee conservation of mass and electric charge. For the present infinitely long cylinder, all variables except ϕ are independent of z, $\mathbf{v} = v_r \hat{\mathbf{r}} + v_\theta \hat{\boldsymbol{\theta}}$, j_z is the only non-zero component of $\mathbf{j}$ and ϕ equals a constant times z. For a long cylinder with electrically insulating ends, such as the crucible bottom, the present two-dimensional solution is realized except near the ends

and the end regions provide the current paths to complete the electrical circuit, provided that there is no net axial current. Here $\mathbf{v}\times\hat{\mathbf{y}}$ is antisymmetric about the $\theta = 0$ plane, so that ϕ is a constant for zero net axial current.

We introduce a streamfunction ψ such that

$$v_r = \frac{1}{r}\frac{\partial\psi}{\partial\theta}, \quad v_\theta = -\frac{\partial\psi}{\partial r}, \tag{2a,b}$$

we substitute the z component of Ohm's law into the momentum equation and we eliminate the pressure in order to obtain a single equation governing ψ,

$$\nabla^2(\nabla^2\psi) = Ha^2(\hat{\mathbf{y}}\cdot\nabla)(\hat{\mathbf{y}}\cdot\nabla\psi), \tag{3}$$

where

$$\nabla^2 = \frac{\partial^2}{\partial r^2} + \frac{1}{r}\frac{\partial}{\partial r} + \frac{1}{r^2}\frac{\partial^2}{\partial\theta^2},$$

$$\hat{\mathbf{y}}\cdot\nabla = \sin\theta\frac{\partial}{\partial r} + \frac{\cos\theta}{r}\frac{\partial}{\partial\theta}.$$

The boundary conditions at the cylinder wall are

$$\psi = 0, \quad \frac{\partial\psi}{\partial r} = -1, \quad \text{at} \quad r = 1. \tag{4}$$

There are two regularity conditions to exclude sources and vortices at $r = 0$, but these are satisfied automatically by our non-singular series solution for ψ. For the present inertialess flow, the streamlines are symmetric about the radii at $\theta = 0$ and at $\theta = \pi/2$, so that we need only consider a quarter of the cylinder with symmetry conditions at $\theta = 0$ and at $\theta = \pi/2$.

We introduce a Fourier series in θ with the appropriate symmetry and we introduce a Chebyshev polynomial series in r. Since the Taylor series of ψ only includes even powers of r, the series is

$$\psi = \sum_{n=0}^{NR}\sum_{m=0}^{N\theta} A_{mn}T_{2n}(r)\cos(2m\theta), \tag{5}$$

where $T_k(r) = \cos[k\arccos(r)]$ is the Chebyshev polynomial of order k. We apply the equation (3) at the Gauss–Lobatto collocation points $r_i = \cos(i\pi/2\text{NR})$ and $\theta_j = j\pi/2N\theta$, for $i = 1$ to $(NR-1)$ and $j = 0$ to $N\theta$, and we apply the boundary conditions (4) at the same values of θ_j. We solve the resultant linear, simultaneous, algebraic equations for the $(NR+1)(N\theta+1)$ values of A_{mn} using Gauss elimination.

The asymptotic solution of the present flow problem for $Ha \gg 1$ was presented by Alemany and Moreau [8] and provides useful insights into our spectral solution for arbitrary values of Ha. For $Ha \gg 1$, the cylinder's interior is subdivided into an inviscid core region, Hartmann layers with $O(Ha^{-1})$ thickness at $r = 1$ and side regions with $\Delta r = O(Ha^{-2/3})$ and $\Delta\theta = O(Ha^{-1/3})$ at $r = 1$ and $\theta = 0$ or π. In the core $\mathbf{v} = O(Ha^{-1})$ and in the Hartmann layers

$$v_{0h} = \exp[Ha|\sin\theta|(r-1)] + O(Ha^{-1}). \tag{6}$$

Neglecting $O(Ha^{-1})$ velocities, only the fluid in the Hartmann layers and side regions rotates with the cylinder, while the core is at rest. Since the Hartmann layer thickness varies as $|\sin\theta|^{-1}$, the total azimuthal flow inside each Hartmann layer or side region is maximum at $\theta = 0$ or π and is minimum at $\theta = \pi/2$ or $3\pi/2$. As θ increases from 0 to $\pi/2$ or from π to $3\pi/2$, fluid must leave each Hartmann layer, and as θ increases from $\pi/2$ to π or from $3\pi/2$ to 2π, an equal amount of fluid must enter each Hartmann layer. The flow circuit is completed by an $O(Ha^{-1})$ velocity along magnetic field lines in the core between the Hartmann layers, so that the core velocity is

$$\mathbf{v}_c = -Ha^{-1}r\cos\theta(1-r^2\cos^2\theta)^{-3/2}\hat{\mathbf{y}} + O(Ha^{-2}). \tag{7}$$

The side regions match the singular core solution (7) as $r \to 1$ for $\theta = 0$ or π and the singular Hartmann layer solution (6) as $\theta \to 0$ or π. Similar side regions have been treated by Roberts [9].

The streamlines from our spectral solution for arbitrary Ha are presented in Fig. 2 for $Ha = 40$ and 200. For $Ha = 0$, the flow is rigid body rotation with $v_r = 0$, $v_\theta = r$, and $\psi = 0.5(1-r^2)$, so that the streamlines are simply concentric circles. For $Ha = 40$, the basic characteristics of the large-Ha solution have emerged but the velocity in the central region is not quite parallel to the magnetic field. The streamlines for $Ha = 200$ match all the characteristics of the large-

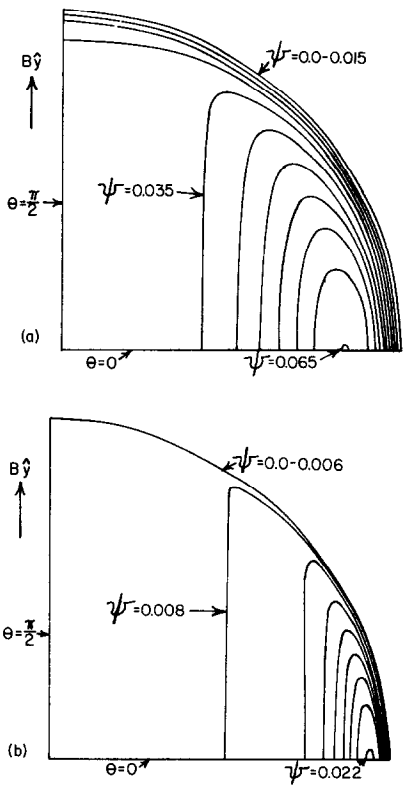

FIG. 2. Streamlines. (a) $Ha = 40$, $\psi = 0.005\,k$, for $k = 0$–13. (b) $Ha = 200$, $\psi = 0.002\,k$, for $k = 0$–11.

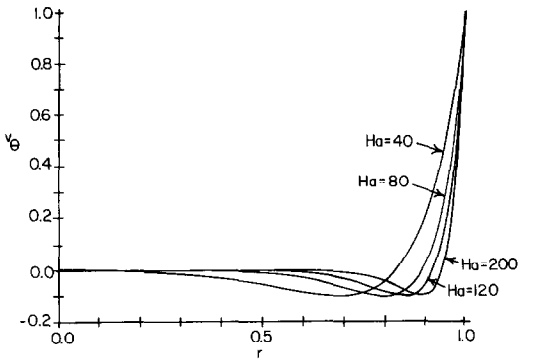

FIG. 3. Azimuthal velocity v_θ vs r at $\theta = 0$ for various values of Ha.

Ha solution and reveal how the side region matches the core velocity to produce a strong circulation for $|r\cos\theta| > 0.8$. The magnitude of the circulation is reflected by the maximum value, ψ_{max}, which decreases as Ha increases. Since all flow must pass through the side region with $\Delta r = O(Ha^{-2/3})$, we expect the circulation to vary as $Ha^{-2/3}$ and indeed ψ_{max} is within 2% of $0.71Ha^{-2/3}$ for all $Ha \geqslant 80$. The values of v_θ at $\theta = 0$ are presented in Fig. 3 for various values of Ha. As Ha increases, the minimum value of v_θ here remains very close to -0.1, so that the large negative values one might expect from the asymptotic solution (7) are never realized. While the arbitrary-Ha solution shares many characteristics with the large-Ha solution, the former serves as a better basis for treating heat and mass transfer since it does not involve the infinite velocities which arise in the asymptotic solution because of the subdivision into separate flow regions.

3. HEAT AND MASS TRANSFER

The streamlines in Fig. 2 indicate that the flow with a transverse magnetic field is far from axisymmetric. In this section we investigate the associated asymmetries in the temperature and solutal distributions for a steady, two-dimensional heat and mass transfer problem with some qualitative similarities to these transfers in Czochralski crystal growth. In an actual Czochralski growth of a silicon crystal, there is a vertical crucible wall at $r = 1$, a horizontal crucible bottom at $z = 0$, a free surface at $z = b$ for $a < r < 1$, and the crystal–melt interface at $z = b$ for $0 < r < a$, where a and b are the dimensionless crystal radius and melt depth, respectively. The crucible bottom is essentially adiabatic, while there is a nearly uniform heat flux into the melt from the vertical crucible wall. For $a < r < 1$, the heat flux is primarily radial, i.e. the isotherms are nearly axial, although there is some axial heat flux associated with the radiation from the free surface. Under the crystal for $0 < r < a$, the heat turns to flow axially into the crystal which represents a thermal sink.

For our two-dimensional heat transfer problem, there is a uniform, radially inward heat flux q at the cylinder wall. For $r < a$, there is a volumetric heat transfer from the liquid equal to a heat transfer coefficient h times the elevation of the dimensional temperature T^* above some reference temperature T_0. This central heat loss corresponds in a very rough way to the heat transfer from the bulk of the Czochralski melt to the crystal, so that T_0 corresponds roughly to the solidification temperature at the crystal face. The dimensionless heat equation is

$$Pe\left(v_r\frac{\partial T}{\partial r} + \frac{v_\theta}{r}\frac{\partial T}{\partial \theta}\right) = \nabla^2 T - BiH(a-r)T, \quad (8)$$

where the dimensionless temperature $T = k(T^* - T_0)/qR$, the Peclet number $Pe = \rho c_h \Omega R^2/k$, and the Biot number $Bi = hR^2/k$, while k and c_h are the thermal conductivity and specific heat of the liquid metal, and $H(x)$ is the Heaviside function. The boundary condition is

$$\frac{\partial T}{\partial r} = 1, \quad \text{at} \quad r = 1, \quad (9)$$

while the exclusion of thermal sources at $r = 0$ is taken care of by our series solution. The temperature is not symmetric about any diameter, but $T(r, \theta+\pi) = T(r,\theta)$, so that we need only consider half the cylinder for $0 \leqslant \theta < \pi$. We again introduce a Fourier series in θ and a Chebyshev polynomial series in r,

$$T = \sum_{n=0}^{(NR-1)} T_{2n}(r)\left[\sum_{m=0}^{(N\theta-1)} B_{mn}\cos(2m\theta) + \sum_{m=1}^{N\theta} C_{mn}\sin(2m\theta)\right].$$

We apply the equation (8) at the same collocation points r_i, θ_j and the boundary condition (9) at θ_j, except now $j = 0$ to $(2N\theta - 1)$, i.e. $0 \leqslant \theta < \pi$. The linear equations for the $2 \times NR \times N\theta$ coefficients B_{mn}, C_{mn} are solved with Gauss elimination.

For our mass transfer problem, we consider a contaminant such as oxygen which enters the liquid metal with a uniform flux q_m at the crucible wall, modelling a uniform ablation rate of the crucible by the melt. For $r < a$, there is a volumetric mass loss equal to a mass transfer coefficient h_m times the elevation of the dimensional concentration C^* above some reference value C_0. Again this roughly models the mass transfer of oxygen from the central melt region to the crystal face. Therefore our mass transfer problem reduces to our heat transfer problem with T replaced by the dimensionless concentration $C = D(C^* - C_0)/q_m R$, with the Peclet number replaced by the mass Peclet number $Pe_m = \Omega R^2/D$ and with the Biot number replaced by the Sherwood number $Sh = h_m R^2/D$, where D is the diffusion coefficient. The only difference between the two problems is that the diffusion coefficients for most dopants and contaminants in silicon are several orders of magnitude smaller than silicon's thermal diffusivity, $k/\rho c_h$, so that the values of Pe_m are generally much larger than those of Pe.

Henceforth we will refer to the lines in the figures as isotherms, but they are also lines of constant concentration for the corresponding mass transfer problem.

For steady-state heat transfer, the average of T for $r < a$ must be $2/a^2Bi$, so that the level of the temperature decreases as Bi increases. The results for $Bi = 0.1$, 1.0 and 10.0, and for several combinations of Ha and Pe indicate that the only essential effect of changing Bi is to change the level of the temperatures and not their distribution. Therefore we only present results for $Bi = 1$, while $a = 0.4$ for all the results presented here. The isotherms for $Ha = 200$ and $Pe = 25$, for $Ha = 200$ and $Pe = 200$, and for $Ha = 40$ and $Pe = 200$ are presented in Fig. 4. The isotherms for $\pi \leqslant \theta < 2\pi$ are obtained by rotating each figure about the origin. For $Ha = 0$, the isotherms are concentric circles corresponding to purely radial conduction through the liquid metal in rigid body rotation. The isotherms for $Ha = 200$ and $Pe = 25$ are still very close to those for $Ha = 0$. For $Ha = Pe = 200$, there is some distortion of the concentric isotherms near $r = 1$ as heat is convected by the flows in opposite directions along the magnetic field lines near $\theta = 0$ and $\theta = \pi$. The isotherms for small values of r are still close to the concentric circles for pure conduction because the fluid here is nearly stagnant, as indicated in Fig. 2(b). For $Ha = 40$ and $Pe = 200$, the isotherms are more distorted from concentric circles because the circulation for $Ha = 40$ is three times as large as that for $Ha = 200$. The isotherms are all skewed to the left by the flows in opposite directions along the magnetic field lines on opposite sides of the radius at $\theta = \pi/2$. In addition, the strong circulations for $|r \cos \theta| > 0.5$ are producing a more uniform temperature region with precisely the distortion of the isotherms one would expect for a strong local circulation.

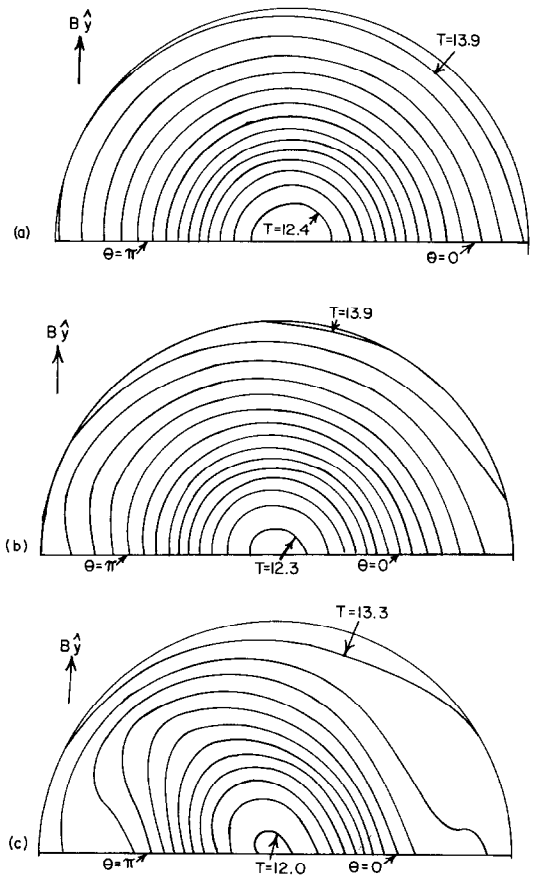

FIG. 4. Isotherms for $Bi = 1.0$, $T = 12.0 + 0.1\ k$ for each case. (a) $Ha = 200$, $Pe = 25$ and $k = 4$–19. (b) $Ha = 200$, $Pe = 200$ and $k = 3$–19. (c) $Ha = 40$, $Pe = 200$ and $k = 0$–13.

4. CONCLUSION

Since the dimensionless circulation actually varies as $Ha^{-2/3}$, ΩR is not the most realistic characteristic velocity for the Peclet number. A more realistic Peclet number would be $Pe' = Pe\,Ha^{-2/3}$, so that $Pe' = 0.731$, 5.848 and 17.10 for the isotherms in Figs. 4(a), (b) and (c), respectively.

Perhaps the most striking aspect of the isotherms in Fig. 4 is that their deviations from the concentric circles for an axisymmetric temperature are smaller than one might expect from the extreme asymmetries in the flow and from the magnitudes of the Peclet numbers. For the heat and mass transfer, there are two competing effects of a transverse magnetic field. Without a magnetic field, the flow and heat transfer are axisymmetric. As the field strength is increased, the flow becomes strongly asymmetric, but it also decreases in magnitude. Once the field strength is sufficiently strong to produce an asymmetric flow, it has also suppressed the flow so much that the flow has relatively little effect on the heat and mass transfer.

A number of experiments have shown that silicon crystals grown by the Czochralski process with a steady, transverse magnetic field have very uniform and controllable concentrations of oxygen and dopants. In addition, the striations produced by the rotation of the crystalizing surface in a slightly asymmetric thermal field are no worse than the corresponding striations in crystals grown without a magnetic field [4]. These experimental results are surprising because one would expect that a transverse magnetic field would produce an extremely asymmetric melt motion, and that the associated convective heat and mass transfer would produce very asymmetric temperature distributions in the melt. Our results demonstrate that the extremely asymmetric melt motions associated with a transverse magnetic field do not necessarily lead to large asymmetries in the temperature and solutal distributions. Clearly our two-dimensional model problems are only qualitative representations of a few physical phenomena also occurring in the complex, three-dimensional melt motion in an actual Czochralski process. Since our results support the promising experimental results for

the Czochralski growth of silicon crystals with a transverse magnetic field, our future research will focus on extensions to more realistic three-dimensional models including the buoyant and thermocapillary convections.

Acknowledgement—This research was supported by the National Science Foundation under Grant CTS-9120448.

REFERENCES

1. E. Kuroda, H. Kozuka and Y. Takano, The effect of temperature oscillations at the growth interface on crystal perfection, *J. Crystal Growth* **68,** 613–623 (1984).
2. A. F. Witt, C. J. Herman and H. C. Gatos, Czochralski-type crystal growth in transverse magnetic fields, *J. Materials Science* **5,** 822–824 (1970).
3. K. M. Kim, Suppression of thermal convection by transverse magnetic field, *J. Electrochemical Society, Solid-State Science and Technology* **129,** 427–429 (1982).
4. P. S. Ravishankar, T. T. Braggins and R. N. Thomas, Impurities in commercial-scale magnetic Czochralski silicon: axial versus transverse magnetic fields, *J. Crystal Growth* **104,** 617–628 (1990).
5. L. N. Hjellming and J. S. Walker, Melt motion in a Czochralski crystal puller with an axial magnetic field: isothermal motion, *J. Fluid Mechanics* **164,** 237–273 (1986).
6. K. Hoshi, N. Isawa, T. Suzuki and Y. Ohkubo, Czochralski silicon crystals grown in a transverse magnetic field, *J. Electrochemical Society, Solid-State Science and Technology* **132,** 693–700 (1985).
7. M. Mihelcic and K. Wingerath, Three-dimensional simulations of the Czochralski bulk flow in a stationary transverse field and in vertical magnetic field: effects on the asymmetry of the flow and temperature distribution in the Si melt, *J. Crystal Growth* **82,** 318–326 (1987).
8. A. Alemany and R. Moreau, Ecoulement d'un fluide conducteur de l'électricité en présence d'un champ magnétique tournant, *J. de Mécanique* **16,** 625–646 (1977).
9. P. H. Roberts, Singularities of Hartmann layers, *Proc. R. Soc. London Ser. A* **300,** 94–107 (1967).